AUTHOR VERSION
Fujii, Y. and Ishijima, Y. (2004), Consideration on Fracture Growth from an Inclined Slit and Inclined Initial Fracture at the Surface of Rock and Mortar in Compression, Int. J. Rock Mech. Min. Sci., Vol. 41, pp. 1035-1041

Consideration on Fracture Growth from Inclined Slit and Inclined Initial Fracture at Surface of Rock and Mortar under Compression

Y. Fujii*, Y. Ishijima

Graduate School of Engineering, Hokkaido University, N13W8. Sapporo, 060-8628, Japan

Key words: Fracture growth; Inclined slit; Initial fracture, Rock; Compression; Numerical simulation

*Corresponding author. Tel./Fax: +81-11-706-6299.

E-mail address: fujii@rock.eng.hokudai.ac.jp (Y. Fujii)

1. Introduction

There have been a number of studies on fracture growth inside rock under compression, and some studies examined near-surface fracture growth [1], [2]. However, fracture growth from an inclined initial fracture at the rock surface would occur much more easily than from a fracture located inside or close to the surface of the rock and such fracture growth would play important roles in spalling of mine pillars, borehole breakout, *etc.* Therefore, the present study was performed to clarify the direction of fracture growth from an inclined slit and an inclined initial fracture at the surfaces of rock and mortar.

A number of theories, such as Sih's maximum tensile stress theory and the maximum energy release rate theory, have been proposed to predict the direction of fracture growth [3]. In Sih's theory, a fracture is assumed to grow at an angle θ_0 given by Eq. (3) when Eq. (1) is satisfied (see Fig. 1 for r and θ).

$$K_{\mathrm{IC}} \le -\sigma_\theta \sqrt{2\pi r} \tag{1}$$

$$\sigma_\theta \sqrt{2\pi r} = -\cos\left(\frac{\theta_0}{2}\right)\left\{K_{\mathrm{I}} \cos^2\left(\frac{\theta_0}{2}\right) - \frac{3}{2} K_{\mathrm{II}} \sin\theta_0\right\} \tag{2}$$

$$\theta_0 = -\left(\frac{K_{\mathrm{II}}}{|K_{\mathrm{II}}|}\right)\cos^{-1}\left(\frac{3K_{\mathrm{II}}{}^2 + K_{\mathrm{I}}\sqrt{K_{\mathrm{I}}{}^2 + 8K_{\mathrm{II}}{}^2}}{9K_{\mathrm{II}}{}^2 + K_{\mathrm{I}}{}^2}\right) \tag{3}$$

where σ_θ is the tangential stress (compression is taken as positive), K_{I} and K_{II} are the stress intensity factors in Mode I and Mode II, respectively, and K_{IC} is the Mode I fracture toughness. The fracture is assumed to

grow perpendicular to the maximum tangential tensile stress. Other theories give similar directions. Such predictions were shown to be effective for homogeneous materials, such as acrylic plates, glass plates, *etc.* [3], [4], and this type of fracture is called a wing crack when it appears in rock under compression. However, the experimental results reported by Bobet & Einstein [5] on rock-type materials showed a different type of fracture growth. They found a crack parallel to the inclined initial slit, as well as wing cracks in compression tests on a gypsum specimen. Vásárhelyi & Bobet [6] carried out a numerical simulation that allowed crack propagation by Mode II as well as wing cracks and their simulation results showed strong agreement with those of experiments. These studies suggest that fracture growth may occur in rock due to shear failure almost parallel to the initial fracture as well as wing cracks, which is fracture growth by tensile failure redacting K_{II}.

Uniaxial compression tests on rock and mortar specimens with an inclined slit from the surface and mortar specimens with an inclined initial fracture from the surface were carried out and fracture growth was observed. A new criterion for fracture growth was introduced in the numerical analysis in the present study to interpret the observed fracture growth.

2. Uniaxial Compression Tests

2.1. Rock Specimen with an Inclined Slit

Rectangular blocks of Shirahama sandstone, measuring 60 × 60 × 120 mm, were made and an inclined slit 1 mm in thickness and 20 mm in length were introduced 50 mm from the lower end. The inclination of the slit from the loading axis was set at 30° for SS30-1 and SS30-2, 45° for SS45-1 and SS45-2, 60° for SS60-1 and SS60-2, and 75° for SS75-1 and SS75-2. Some mechanical properties of the Shirahama sandstone are shown in Table 1. The specimens were then compressed uniaxially at a platen displacement speed of 0.1 mm/s using an Instron 5586 mechanical loading frame, with a maximum capacity of 300 kN. Axial load was increased to between 25 and 50 MPa until visible fracture growth occurred and the load was released.

No clear relationship was observed between the load at which the main fracture initiated and the inclination of the slit. More than one fracture was observed at the tip of the slit (Fig. 2) and one of the fractures (main fracture) grew upward (Fig. 3). The main fracture was considered to have initiated mainly

due to shear slip as it initiated from the corner at which the compressive stress was concentrated. All main fractures curved slightly to the free surface. The tip of the slit was crushed and this phenomenon was clearly observed for the largest inclination (ss75-1, 2).

2.2. Mortar Specimen with an Inclined Slit

Portland cement, silica sand, and water were mixed at a 3:6:2 weight ratio. The mixture was poured into a rectangular steel mold measuring 60 × 60 × 120 mm and removed 24 hours later. The mortar block was cured in water for two weeks and then stored in the laboratory. Some of the mechanical properties of the mortar block are shown in Table 1. An inclined slit was introduced similarly to the sandstone specimens. The angle of the slit was 30° (m30), 45° (m45), 60° (m60), or 75° (m75). Uniaxial compression tests were carried out in a manner similar to that described in the previous section. The specimens after the tests are shown in Fig. 4. Both m30 and m60 showed fractures with a small initiation angle. A fracture with a large initiation angle was found in m75. The downward fracture growth in m45 was categorized as an oblique secondary crack according to Sagong & Bobet [7], and the mechanism should be investigated in future studies. All of the fractures curved slightly toward the free surface.

2.3. Mortar Specimen with an Inclined Initial Fracture

Mortar blocks of 205 × 205 × approx. 50 mm were made as described in the previous section. A steel wedge was impacted against the mortar blocks to create initial fractures (Fig. 5). The mortar blocks were then cut to make specimens with an inclined initial fracture. The specimens had different sizes, as shown in Table 2, as a result of the method of preparation. The uniaxial compression tests were carried out in a manner similar to that described in the previous section. Photographs of the specimens after the tests, each showing the fracture clearly, are shown in Fig. 6. The fractures grew almost parallel to the direction of the initial fractures.

3. Simulation of Fracture Growth

3.1. Analysis based on Sih's maximum tensile stress theory

The simulation was based on stress analysis by the displacement discontinuity method (DDM) [8]. DDM is an indirect type of boundary element method in which the boundaries and fractures are divided into displacement discontinuity elements. Fracture growth is thus simulated by addition of a displacement discontinuity element to the fracture tip. This is different from FEM analysis in which fracture growth is usually simulated as an element failure or a separation of element nodes. The simulation was performed as follows (Fig. 7).

(i) Elastic stress analysis was carried out using DDM.

(ii) The stress intensity factor for all fracture tips was evaluated using the following formulae [3]:

$$K_{\mathrm{I}} = \sqrt{\frac{2\pi}{r_{\mathrm{B}}}} \frac{G}{\kappa + 1} [b_y] \tag{4}$$

$$K_{\mathrm{II}} = \sqrt{\frac{2\pi}{r_{\mathrm{B}}}} \frac{G}{\kappa + 1} [b_x] \tag{5}$$

where K_{I} and K_{II} are the stress intensity factors in Modes I and II, respectively, G is the rigidity, r_{B} is the distance between the fracture tip and the point B near the fracture tip (Fig. 8), and $[b_x]$ and $[b_y]$ are the shear and opening components of the displacement discontinuity at point B, respectively,

$$\kappa = 3 - 4\nu \tag{6}$$

for the plane strain condition and

$$\kappa = \frac{3 - \nu}{1 + \nu} \tag{7}$$

for the plane stress condition. A plane strain condition was assumed and the center of the tip element was regarded as point B in the present study.

(iii) Sih's maximum tensile stress theory [3] was assumed as the criterion for fracture growth and a search began for the element at which the value of the right-hand side of Eq. (2) was maximized.

(iv) A new displacement discontinuity element at an angle given by Eq. (3) was added when Eq. (1) is satisfied by the element found in the previous step.

(v) Steps (i) to (iv) were iterated until fracture growth stopped.

(vi) Step (v) was iterated incrementally approaching the boundary conditions. Analysis was stopped when all fracture tips crossed the model boundary.

The stress intensity factor obtained by DDM using the constant displacement discontinuity elements was

overestimated even if the elements were sufficiently small. To overcome this shortcoming, a shorter element was used for the fracture tip and $r_{B'}$ was used instead of r_B to evaluate the stress intensity factor (Fig. 8). The length of the tip element was determined to be 0.75 times the other elements by comparing the theoretical solutions and the calculated results. The error in the stress intensity factor was less than 10% with 4 or more elements for a fracture under tension at an infinite distance or with 10 or more elements for a fracture with a pair of point forces at its center (Fig. 9).

3.2. The new criterion

Fracture growth due to shear failure, as well as tensile failure propagation, was allowed in the new criterion. K_I and K_{II} calculated using Eqs. (4) and (5) were substituted into Eqs. (2) and (8), and $\sqrt{2\pi r}$ times the stress components was evaluated (compressive stress was still taken as positive).

$$\tau_{r\theta}\sqrt{2\pi r} = -\cos\frac{\theta}{2}\{K_I \sin\theta + K_{II}(3\cos\theta - 1)\} \tag{8}$$

From those stress components, the maximum value of

$$K_T = -\sigma_\theta \sqrt{2\pi r} \tag{9}$$

and the angle θ_T at which K_T becomes the maximum were calculated. Similarly, the maximum value of

$$K_S = (|\tau_{r\theta}| - \sigma_\theta \tan\phi_S)\sqrt{2\pi r} \tag{10}$$

and the angle θ_S at which K_S becomes the maximum were calculated. In Eq. (10), ϕ_S is a newly introduced physical quantity called the microscopic internal friction angle. This quantity represents the internal friction angle in the vicinity of the fracture tip and does not have to be identical to the internal friction angle in Coulomb's criterion for the material. A new element is added at the angle θ_T when K_T is larger than K_{IC}. The same solution as Sih's maximum tensile stress theory was obtained in this case. On the other hand, a new element at the angle θ_S is added when K_S is bigger than K_{IIC}, which is Mode II fracture toughness, to account for shear-type fracture growth.

3.3. Simulation results

Tests on Shirahama sandstone were simulated using the model shown in Fig. 10. Young's modulus, Poisson's ratio, and Mode I fracture toughness in Table 1 were used. K_{IIC} was not measured so that its value

was assumed to be the same as K_{IC}. Axial stress up to 29 MPa was applied incrementally in 1 MPa steps. The slit was modeled by an open initial fracture, *i.e.*, a traction-free condition was assumed at the surfaces of the initial fracture. The friction angle between the added closed fracture elements was assumed to be 30°.

Based on the results of Sih's theory (Fig. 11), the fracture did not grow at all or initiated at a large angle from the tip of slit and stopped after only a short interval. On the other hand, in the present method, shear-type upward fracture growth was obtained. The angle at the initiation was relatively small and the fracture curved slightly toward the free surface. These features agreed with the observations. The best agreement was obtained when the angle of microscopic internal friction was set at 5°. The proposed method was better than that reported by Vásárhelyi & Bobet [6] as in their method fractures cannot curve. Similar results were expected for mortar specimens.

Simulation for mortar specimens with an initial closed fracture inclined at 30° to the loading axis was also carried out in a similar manner as for the slit using the mechanical properties of the mortar specimens. Upward fracture growth was observed in all cases and the fracture growth angle was even smaller than in the cases with a slit. However, long main fractures were not observed in the prediction by Sih's method. The geometries of the grown fractures determined by the proposed method agreed with the experimental results much more closely than those obtained by Sih's method. To which theory the growth behavior is most similar would depend on the ratio of the tensile to shear strength in the vicinity of the fracture tip.

5. Conclusions

Compression tests on rock and mortar specimens with an inclined slit from the specimen surface or an inclined initial fracture from the specimen surface were performed. The observed fracture growth was numerically simulated employing a new criterion. The main results were as follows.

(1) The fracture from the inclined slit from the specimen surface grew at a small angle to the initial direction and curved slightly towards the free surface in all cases for rock specimens and in two of four cases for mortar specimens.

(2) The fracture from the inclined initial fracture from the surface of mortar specimens grew almost parallel to the initial fracture.

(3) Simulation employing the proposed method, which considers shear fracture growth as well as tensile growth, gave much better results than the widely used Sih method.

Some problems remain to be resolved in the method described here. The present method is empirical and the physical significance of ϕ_S is not yet clear. Continued improvement of this method will allow more practical analysis of fracture growth in rock and rock masses.

References

[1] Vardoulakis, I, Papamichos, E. Surface Instabilities in Elastic Anisotropic Media with Surface-parallel Griffith Cracks, Int. J. Rock Mech. Min. Sci. & Geomech. Abstr. 1991:28(2/3):163-171

[2] Germanovich, LN, Roegiers, JC. A Model for Borehole Breakouts in Brittle Rocks, Rock Mechanics in Petroleum Engineering (Proc. Eurock '94), Balkema, Rotterdam.1994:361-370

[3] Ingraffea AR. Numerical Modeling of Fracture Propagation, Rock Fracture Mechanics, ed. by Rossmanith, HP, Springer - Verlag, Wien - New York;1983: 151-208.

[4] Nemat-Nasser S, Horii H. Compression-induced Nonplanar Crack Extension with Application to Splitting, Exfoliation, and Rockburst, J. Geophys. Res. 1982;87(B8):6805-6821.

[5] Bobet A, Einstein HH. Fracture Coalescence in Rock-type Materials under Uniaxial and Biaxial Compression, Int. J. Rock Mech. Min. Sci. & Geomech. Abstr. 1998;35(7):863-888.

[6] Vásárhelyi B, Bobet A. Modeling of Crack Initiation, Propagation and Coalescence in Uniaxial Compression, Rock Mech. Rock Engng. 2000;33(2):119-139.

[7] Sagong M, Bobet A. Coalescence of Multiple Flaws in a Rock-model Material in Uniaxial Compression, Int. J. Rock Mech. Min. Sci. 2002;39(2):229-241.

[8] Crouch SL, Fairhurst C. The Mechanics of Coal Mine Bumps and the Interaction between Coal Pillars, Mine Roof and Floor, U.S.B.M. Contract Report, H0101778; 1973.

Table 1

Mechanical properties of the specimens. Data are given as "value ± standard deviation (number of specimens)". Critical compressive/extensile strains are defined as axial/circumferential strain values at peak load points in uniaxial compression tests, respectively.

Physical properties	Shirahama sandstone	Mortar
Bulk density (10^3 kg/m^3)	2.24 (1)	---
P-wave velocity (km/s)	2.33 (1)	---
Young's modulus (GPa)	11.5±0.3 (5)	14.2±1.1 (5)
Poisson's ratio	0.47±0.05 (5)	0.10±0.05 (5)
Uniaxial compressive strength (MPa)	60.0±1.5 (5)	38.8±0.8 (5)
Critical compressive strain (%)	0.826±0.04 (5)	0.399±0.058 (5)
Critical extensile strain (%)	-0.506±0.08 (5)	-0.146±0.010 (5)
Indirect tensile strength (MPa)	2.61 (1)	3.07±0.34 (5)
Mode I Fracture toughness (MPa m$^{0.5}$)	0.553±0.01 (2)	0.610±0.082 (6)

Table 2

Dimensions of mortar specimens each with an initial fracture

Sample No	Height (mm)	Width (mm)	Thickness (mm)	Crack height (mm)
m11	101.5	51.2	44.5	2.0
m12	86.9	38.9	46.6	15.0
m13	108.3	56.3	47.8	20.0
m14	99.5	46.6	50.2	15.0
m15	93.8	54.9	49.2	3.0
m16	72.7	43.1	51.9	11.5
m17	83.4	40.9	51.0	9.5
m18	70.2	55.9	51.9	17.0

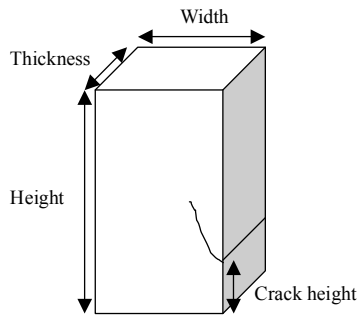

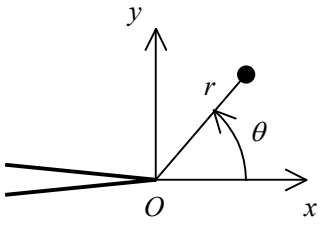

Fig. 1. Coordinate in the vicinity of fracture tip.

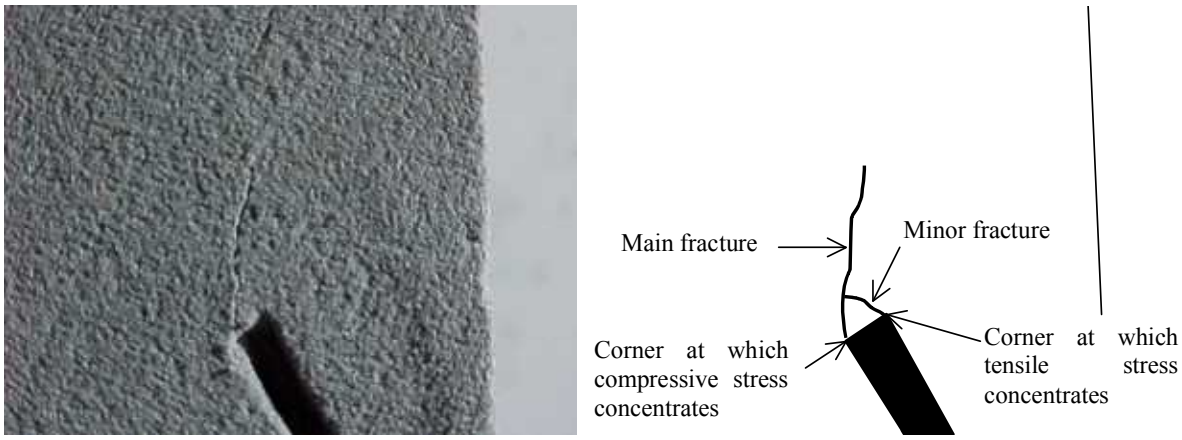

(a) (b)

Fig. 2. (a) : Magnified photograph of the slit end of ss30-2. (b): schematic figure showing explanations

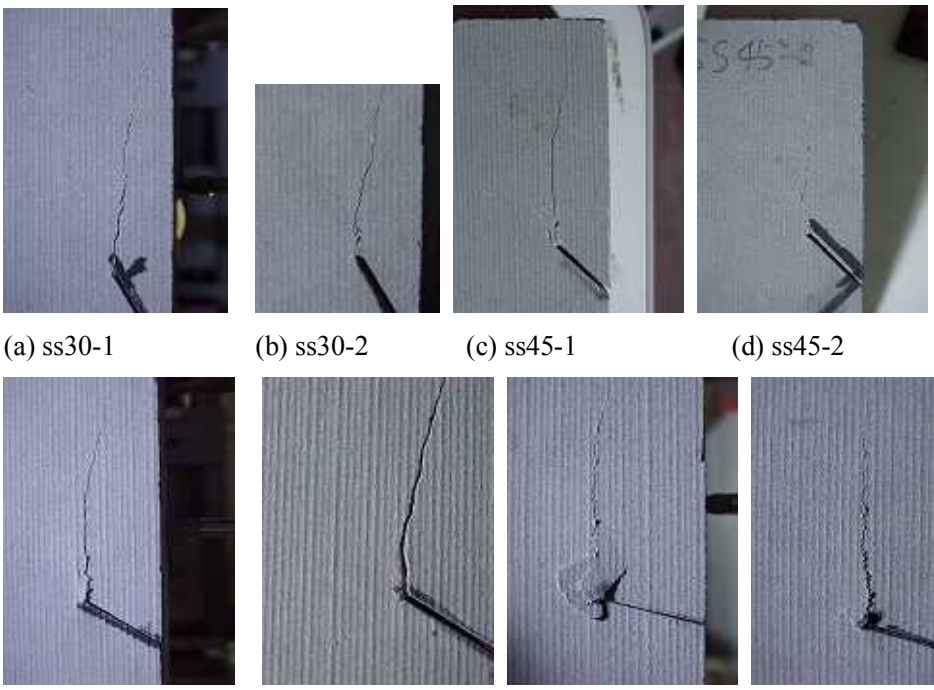

(a) ss30-1 (b) ss30-2 (c) ss45-1 (d) ss45-2

(e) ss60-1 (f) ss60-2 (g) ss75-1 (h) ss75-2

Fig. 3. Specimens of Shirahama sandstone having an inclined slit with varied inclination. Photographs except for (d) are reversed.

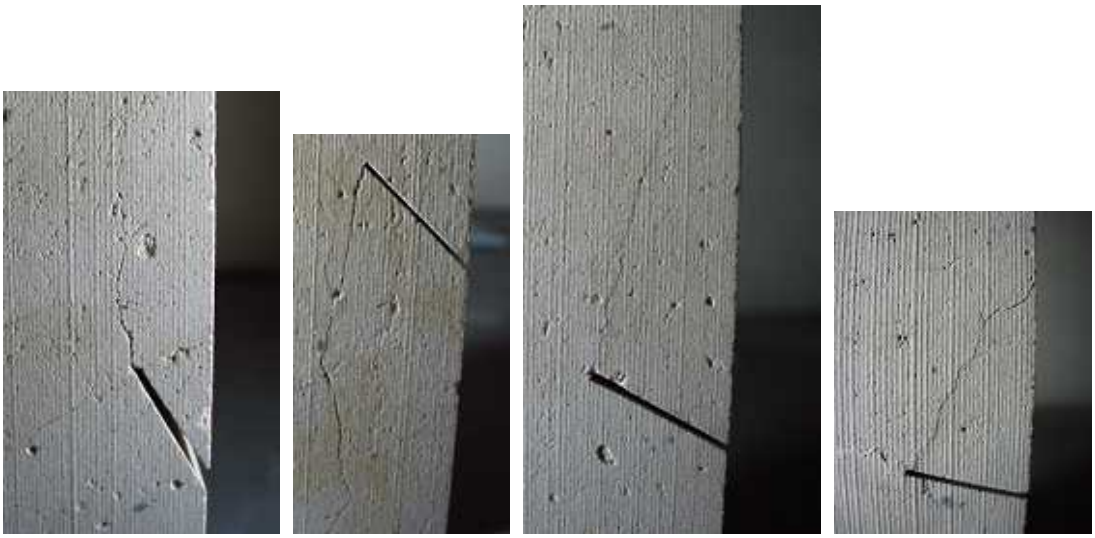

(a) m30 (b) m45 (c) m60 (d) m75

Fig. 4. Mortar specimens having an inclined slit after tests. (a) is reversed.

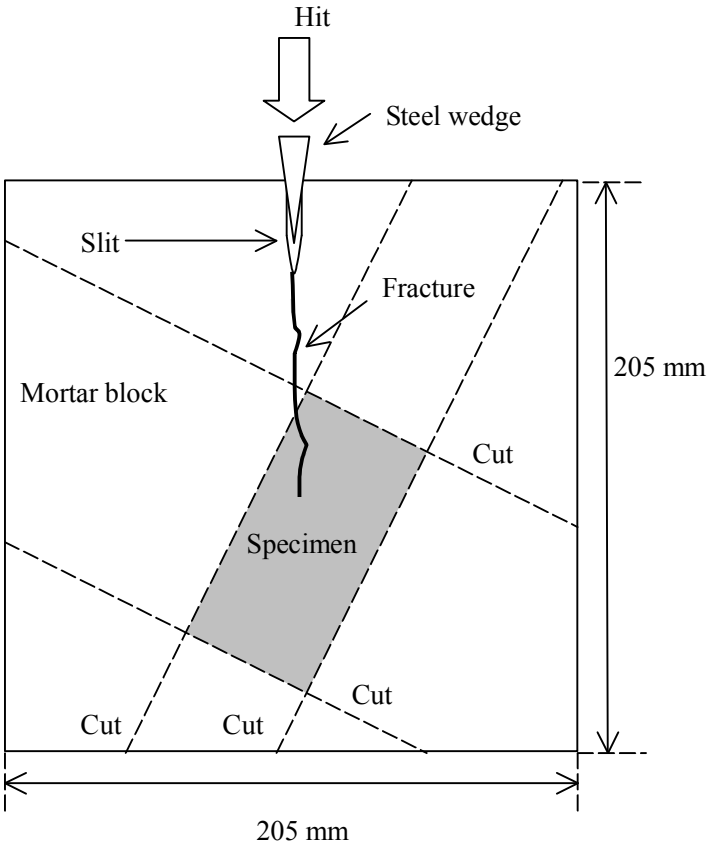

Fig. 5. Schematic figure showing preparation of mortar specimen with an inclined initial fracture

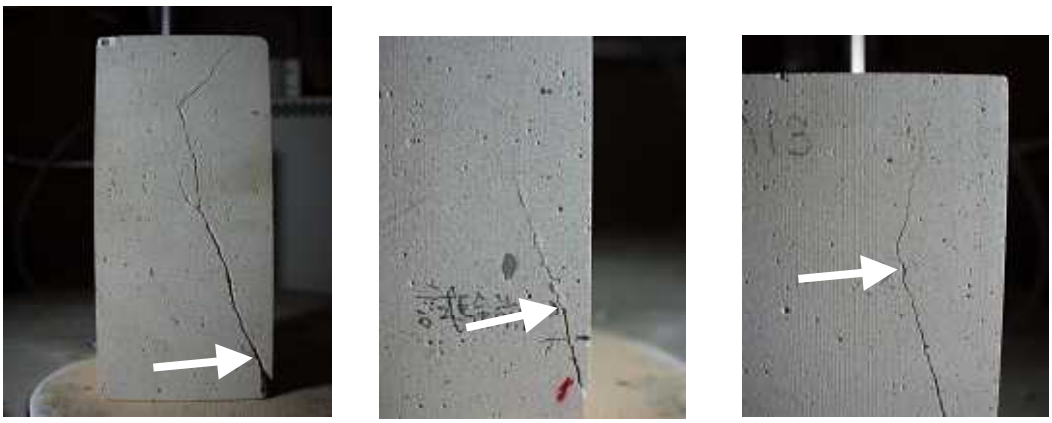

(a) M11 (b) M12 (c) M13

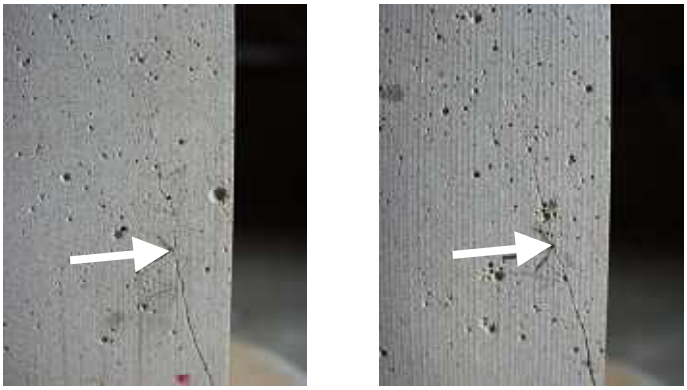

(d) M17 (e) M18

Fig. 6. Mortar specimens with an inclined initial fracture after testing. Arrows show the initial fracture tips that were determined by the naked eye before loading. (a) is reversed.

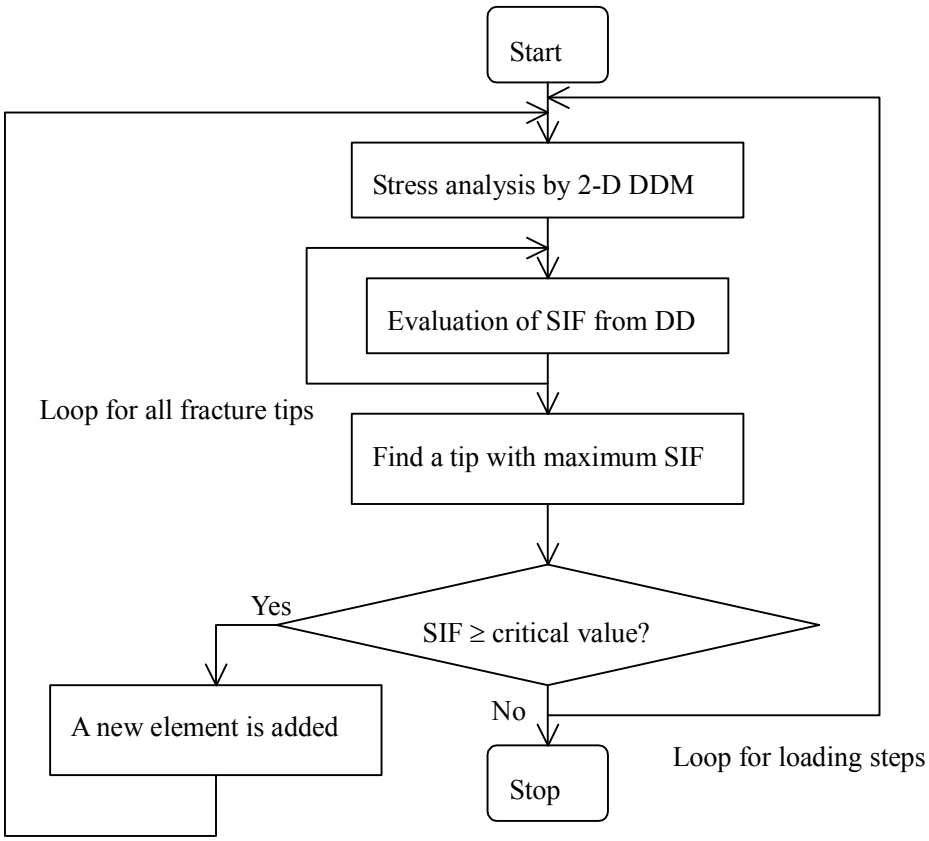

Fig. 7. Flow chart of numerical simulation for fracture growth. SIF, 2-D DDM and DD represent stress intensity factor, two dimensional displacement discontinuity method and displacement discontinuity, respectively.

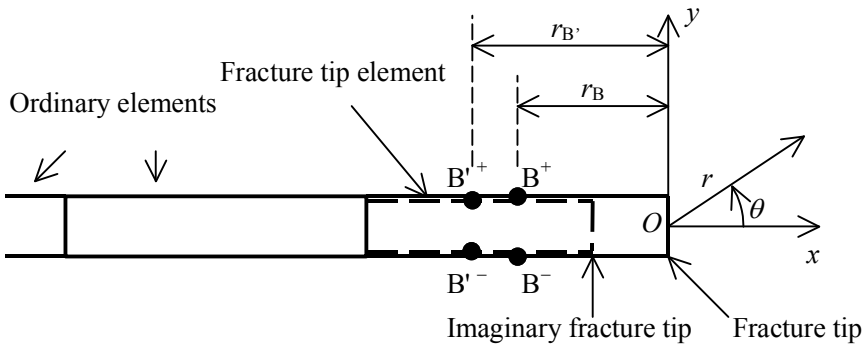

Fig. 8. Element for fracture tip is shown. Displacement discontinuity at point B' was used to evaluate stress intensity factor K_I and K_{II}, and the angle of fracture growth instead of that at point B.

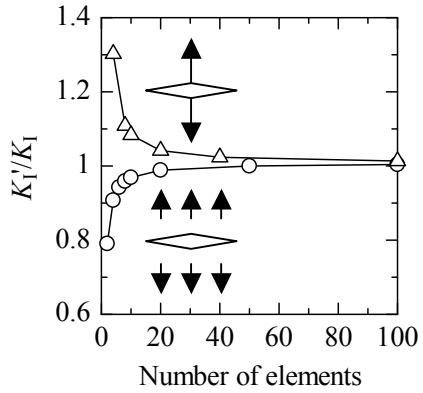

Fig. 9. Stress intensity factor K_I', which was evaluated with displacement discontinuity method and normalized by analytical solution K_I, for a fracture under tensile stress at infinite distance (open circles) and a fracture which is subjected to a pair of point loads at its center (open triangles).

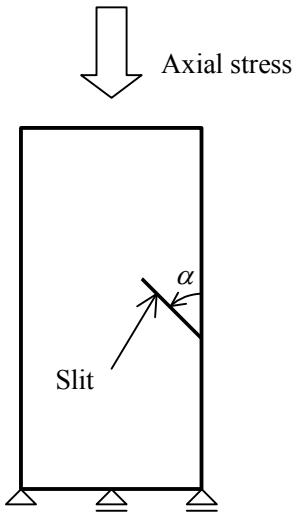

Fig. 10. Model used in the simulation

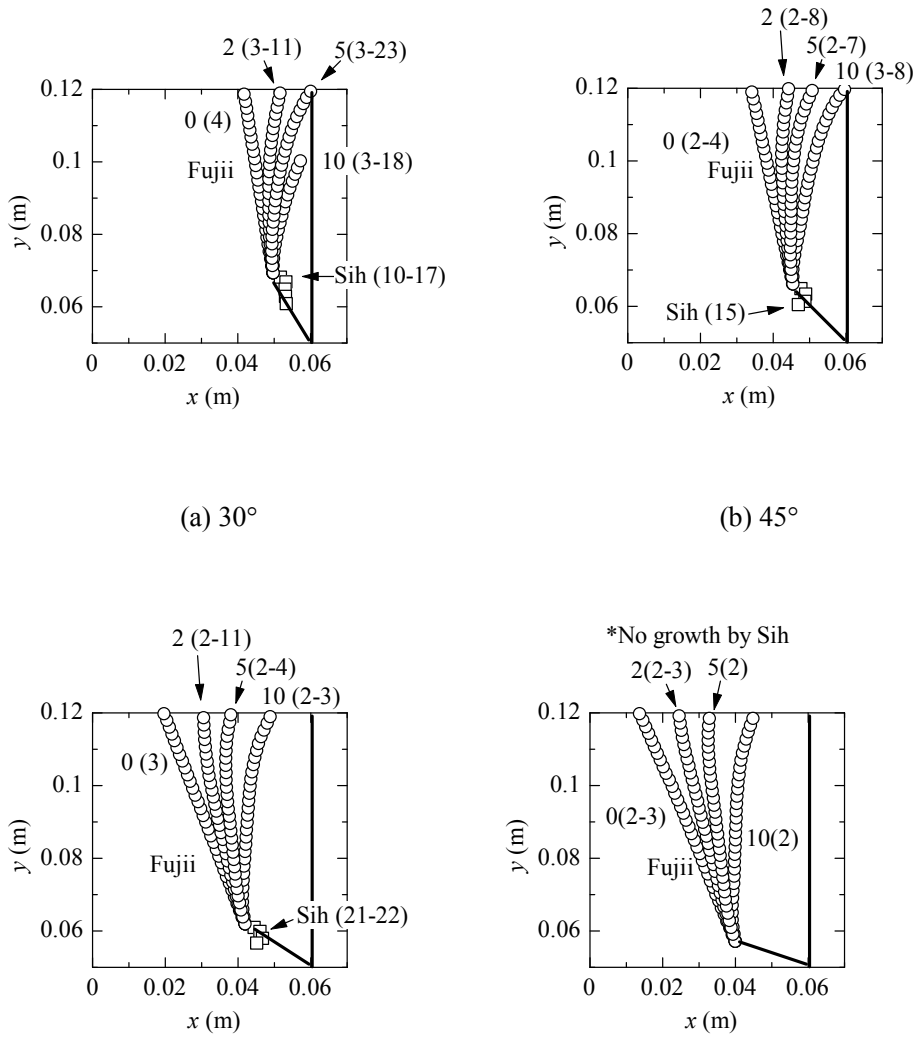

(a) 30° (b) 45°

(c) 60° (d) 75°

Fig. 11. Results of numerical simulation for fracture growth from inclined slit for Shirahama sandstone specimen. 'Sih' is based on Sih and 'Fujii' is based on the proposed method. Numerals 0, 2 and 10 denote the angle of internal friction in degree for the proposed method. Numerals in parentheses denote the applied axial stress in MPa. For example, (2) means that the fracture grew when the applied stress reaches 2 MPa and (3-13) means that the fracture began to grow when the applied stress reached 3 MPa and continued to grow until the applied axial stress reached 13 MPa.

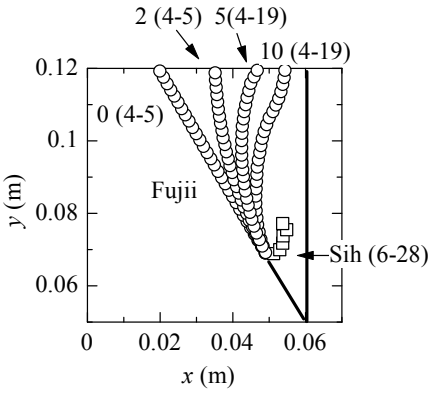

Fig. 12 Results of numerical simulation for fracture growth from inclined initial fracture of mortar specimen. The inclination of the initial fracture was set at 30°.